Undecimated Dual Tree Complex Wavelet Transforms

Paul Hill, *Member, IEEE,* Alin Achim, *Member, IEEE,* and David Bull, *Fellow, IEEE*

***Abstract*—Two undecimated forms of the Dual Tree Complex Wavelet Transform (DT-CWT) are introduced and their application to image denoising is described. These undecimated transforms extend the DT-CWT through the removal of downsampling of the filter outputs together with upsampling of the filters in a similar structure to the Undecimated Discrete Wavelet Transform (UDWT).**

Both the developed transforms offer exact translational invariance, improved scale-to-scale coefficient correlation together with the directional selectivity of the DT-CWT.

Additionally, within each of these developed transforms, the subbands are of a consistent size. They therefore benefit from a direct one-to-one relationship between co-located coefficients at all scales. This is an important relationship that can be exploited within applications such as denoising, image fusion and segmentation.

The enhanced properties of the transforms have been exploited within a bivariate shrinkage denoising application, demonstrating quantitative improvements in denoising results compared to the DT-CWT. The two novel transforms together with the DT-CWT offer a trade off between denoising performance, computational efficiency and memory requirements.

***Index Terms*—Discrete wavelet transforms, Image denoising**

I. Introduction

THE Discrete Wavelet Transform (DWT) is a spatial-frequency transform that has been used extensively for analysis, denoising and fusion within image processing applications. It has been recognised that although the DWT gives excellent combined spatial and frequency resolution, the DWT suffers from shift variance[1], [2], [3]. Various adaptations to the DWT have been developed to produce a shift invariant form. Firstly, an exact shift invariance has been achieved using the Undecimated Discrete Wavelet Transform (UDWT). However, the UDWT variant suffers from a considerably over-complete representation together with a lack of directional selectivity. More recently, the Dual Tree Complex Wavelet Transform (DT-CWT) has given a more compact representation whilst offering near shift invariance. The DT-CWT also offers improved directional selectivity (6 directional subbands per scale) and complex valued coefficients that are useful for magnitude / phase analysis within the transform domain. This paper introduces two undecimated forms of the DT-CWT which combine the benefits of the UDWT (exact translational invariance, a one-to-one relationship between all co-located coefficients at all scales) and the DT-CWT (improved directional selectivity and complex subbands).

Department of Electrical and Electronic Engineering, University of Bristol, Bristol, BS8 1UB, UK e-mail: (paul.hill@bristol.ac.uk)

Manuscript received ?; revised ?

Firstly, the filter structure of the UDWT is introduced within section II. This filter structure is then applied to the DT-CWT decomposition to give the two forms of the undecimated DT-CWT as described within sections III and IV. The shift invariance, generalisation to two dimensions and cross scale correlation of the developed transforms are then investigated in sections V, VI and VII respectively. The implemented denoising algorithm as applied to the new transforms is described in sections VIII, IX and IX-A. Finally, the results, a comparison of transforms and conclusion are presented in sections XI, XII and XIII respectively.

II. The Undecimated Discrete Wavelet Transform (UDWT)

The Undecimated Discrete Wavelet Transform has been independently developed by numerous researchers separately defined by a number of names including "algorithme a trous [2]", "the Shift Invariant DWT (SIDWT) [1]", and "Discrete Wavelet Frames (DWFs) [3]".

Defining the scaling and wavelet filters of an orthonormal DWT as $h \in \ell^2(\mathbb{Z})$ and $g \in \ell^2(\mathbb{Z})$ respectively. The undecimated wavelet filter at scale l+1 is defined recursively as

$$g^{(l+1)}[k] = g^{(l)}[k] \uparrow 2 = \begin{cases} g^{(l)}\left[\frac{k}{2}\right], & \text{if } k \text{ even} \\ 0, & \text{if } k \text{ odd.} \end{cases} \quad (1)$$

The down sampling at each stage of the DWT is removed to give the UDWT. The shift variation of the DWT is caused by this subsampling and it's removal within the UDWT provides perfect shift invariance. Furthermore, each subband is now the same size as the original signal leading to a considerably over-complete representation.

III. The Undecimated dual tree complex wavelet transform type 1: U1DT-CWT

The UDWT does not use any down sampling and therefore is exactly shift invariant. However, it lacks directionality and has only real coefficients for analysis and processing. Kingsbury [4] has formulated The Dual Tree Complex Wavelet Transform (DT-CWT) to provide near shift invariance and improved directionality within a more compact representation. The structure of the DT-CWT uses two separate trees to form Hilbert filter pairs within each subband. The magnitude response of this pair of filters is very near to being shift invariant. Another benefit of this transform is improved directional resolution (in the two dimensional version). The near shift invariance and improved directional selectivity have facilitated excellent results in denoising, fusion and other image processing applications.

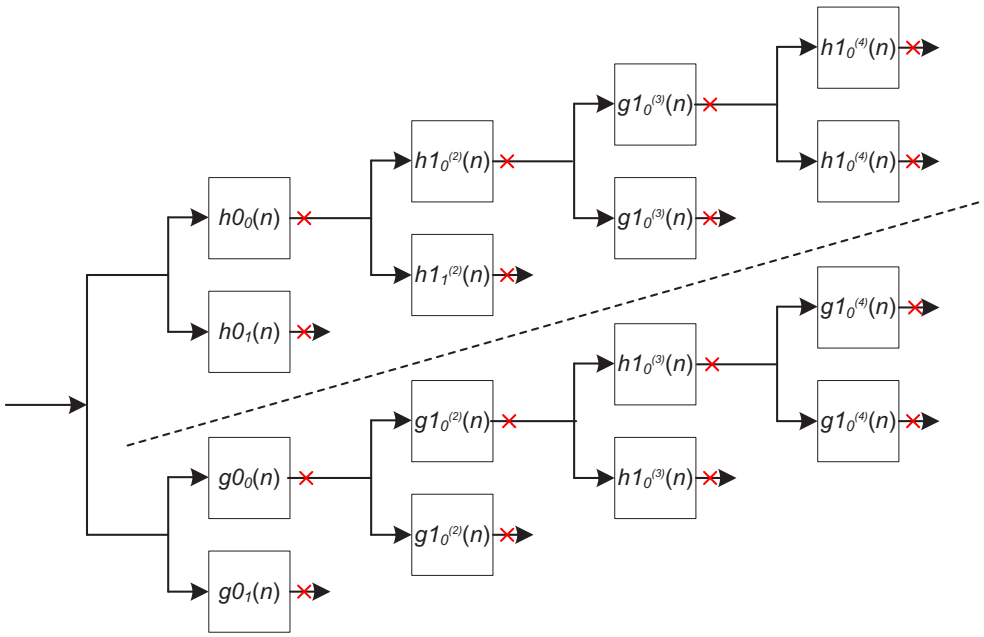

Fig. 1. The analysis stage of the U1DT-CWT. The crosses indicate the positions where downsampling would normally occur within the decimated DT-CWT.

In common with conventional wavelet transforms, the size of the subbands in the DT-CWT decreases in octaves as the scale of the transform increases in order to provide optimal resolution / redundancy at each level. However, this leads to an approximate relationship between co-located coefficients across scales. Cross scale relationships are exploited in segmentation, fusion and denoising applications (e.g. [5][6]). The correlation between a coefficient and it's parent is exploited within each of these application.

Although subsampling is justified for compression applications, the subsampled subbands of the DT-CWT have a restricted number of coefficients directly related to each spatial position in the signal or image: a relationship that is often required within analysis applications [6].

To enable such analysis we now define the first undecimated form of the DT-CWT: the U1DT-CWT where each subband has the same resolution as the signal. As the U1DT-CWT contains no subsampling it exhibits perfect shift invariance. It also offers a one-to-one relationship between all co-located coefficients and the original samples and also between co-located coefficients.

The U1DT-CWT analysis stage is shown in figure 1. Filters at each stage are based on the filters used in the DT-CWT.

- Any perfect reconstruction bi-orthogonal set of filters can be used for the first level. The filters of one tree ($g0_0$, $g0_1$) are exactly the same as the other tree ($h0_0$, $h0_1$) but offset by one sample. As they are the first level, these filters are not upsampled (they do not need to take into account a previous level's subsampling).
- All subsequent filters in both trees are based on the q-step filters defined in [4].

The subsampling of the DT-CWT has been removed as indicated by the crosses in figure 1. To offset this effect at the next and subsequent levels each of the q-step filters is itself upsampled (i.e. zeros are inserted between filter coefficients). For example the q-step filter $g1_0$ the U1DT-CWT filter at stage $l+1$ is defined recursively (as within UDWT) as

$$g1_0^{(l+1)}[k] = g1_0^{(l)}[k] \uparrow 2 = \begin{cases} g1_0^{(l)}\left[\frac{k}{2}\right], & \text{if } k \text{ even} \\ 0, & \text{if } k \text{ odd} \end{cases} \quad (2)$$

where $g1_0^{(1)}$ is the original (non upsampled) q-step filter. The other upsampled filters (at stage $l+1$: $g1_0^{(l+1)}$, $h1_0^{(l+1)}$ and $h1_1^{(l+1)}$) in figure 1 are similarly defined (and all subsequenct stages). The synthesis stage of the whole transform is the inverse of figure 1 transformed with similarly upsampled filters resulting in perfect reconstruction.

IV. The Undecimated Dual Tree Complex Wavelet Transform Type 2: U2DT-CWT

The removal of all subsampling from the U1DT-CWT compared to the DT-CWT leads to a transform that has perfect shift invariance, improved subband to subband correlation but is extremely overcomplete. We now identify that retaining the first level of subsampling also provides perfect shift invariance while significantly reducing overcompleteness.

Taking the first level high-pass filter of the DT-CWT to be g. The real and imaginary outputs ($y_{\Re}$ and $y_{\Im}$ respectively) can be defined as given in equations 3 and 4. This shows that the same filter is used but is offset by one sample to generate each component. Each complex coefficient $y[n]$ is defined as given in equation 5.

$$y_{\Re}[n] = \sum_k g[k] \cdot x[2n-k] \quad (3)$$

$$y_{\Im}[n] = \sum_k g[k] \cdot x[2n-k+1] \quad (4)$$

$$(y[n])^2 = |y_{\Re}[n] + iy_{\Im}[n]| = (y_{\Re}[n])^2 + (y_{\Im}[n])^2 \quad (5)$$

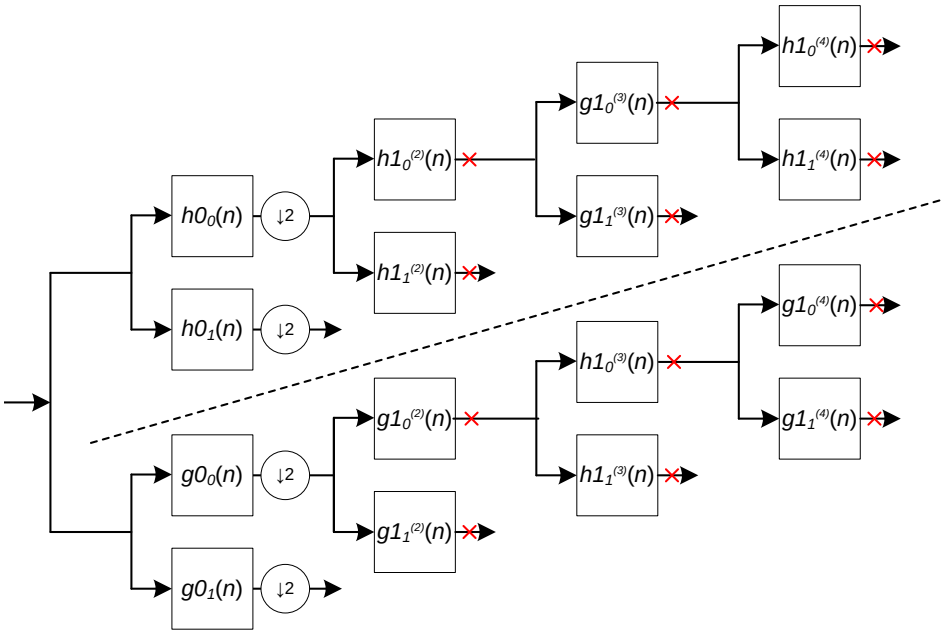

Fig. 2. The analysis stage of the U2DT-CWT. The crosses indicate the positions where downsampling would normally occur within the decimated DT-CWT.

Shifting the input signal x by one sample gives a new complex output y_d defined by equations 6, 7 and 8. This equates to a summation of the original unshifted components $y_{\Re}$ and $y_{\Im}$ as illustrated by equation 8.

$$y_{d_{\Re}}[n] = \sum_k g[k] \cdot x[2n-k+1] = y_{\Im}[n] \tag{6}$$

$$y_{d_{\Im}}[n] = \sum_k g[k] \cdot x[2n-k+2] = y_{\Re}[n+1] \tag{7}$$

$$(y_d[n])^2 = |y_{d_{\Re}}[n] + i y_{d_{\Im}}[n]| = (y_{\Im}[n])^2 + (y_{\Re}[n+1])^2 \tag{8}$$

The energy of this subband is defined as the summation of $y[n]$ over the signal.

$$\begin{aligned} E &= \textstyle\sum_n (y[n])^2 = \sum_n (y_{\Re}[n])^2 + (y_{\Im}[n])^2 \\ E_d &= \textstyle\sum_n (y_d[n])^2 = \sum_n (y_{\Im}[n])^2 + (y_{\Re}[n+1])^2 \end{aligned} \tag{9}$$

$\therefore$ discounting any boundary effects any shift d will still result in perfect shift invariance i.e. $E = E_d$.

If the subsequent levels are not subsampled then the lower scale subbands will also exhibit perfect shift invariance. This transform is the second undecimated DT-CWT termed: U2DT-CWT (illustrated by figure 2). The perfect shift invariance of the U2DT-CWT is illustrated in table III

The U2DT-CWT gives all subbands that are the same size (vital for the use of cross scale coefficient correlation), but half the size of the input signal leading to a significant reduction in overcompleteness.

V. Evaluation of Shift Invariance

In order to evaluate the shift invariance of each wavelet transform we define a finite length 1D step signal

$$x_d[n] = \begin{cases} 0, & 0 \le n < d + N/2 \\ 1, & d + N/2 \le n \le N \end{cases} \tag{10}$$

A detail subband output of the chosen wavelet transform at level s can be represented by the multiplication of the signal by the transform matrix (W_s).

$$y_{d_s} = W_s x_d \tag{11}$$

$$E_{d_s} = \textstyle\sum (y_{d_s})^2 \tag{12}$$

A series of energy measures of the detail subband is generated by varying the displacement of the step signal using d from 0 to M (where M$\ll$N).

$$E_{d_s} = \textstyle\sum (y_{d_s})^2, \quad d = 0 \ldots M-1 \tag{13}$$

The variation of E_d therefore represents the degree of shift variance. Although the natural measure of shift invariance would be the coefficient of variance (σ/μ) the degree of shift invariance has been defined by Adam et al. [7] as

$$\text{Deg} = 1 - \frac{\sigma}{\mu} \tag{14}$$

We define the length of the signal to be 1024 (i.e. N = 1024) and the number of offset steps to 16 (i.e. M = 16). The degree of shift invariance (Deg) was obtained for the first four high pass subbands of the 1D DWT, DT-CWT, U1DT-CWT and U2DT-CWT transforms. For the complex transforms (the non DWT transforms) Deg was obtained for the real, imaginary and magnitude of the subbands. These results are shown in figure I. This table shows the improved shift invariance of the DT-CWT compared to the DWT (especially the magnitude). The U1DT-CWT offers perfect translational invariance for all scales and all components. Furthermore, the U2DT-CWT offers perfect translational invariance for the coefficient magnitudes for all scales (explained by the analysis given by equations 6-9).

VI. Two Dimensional U1DT-CWT and U2DT-CWT Transforms

Through separable application of the one dimensional DT-CWT in the horizontal and vertical directions on an image a two dimensional DT-CWT is created. This transform creates 6 oriented complex subbands at each scale. Similarly the one dimensional U1DT-CWT and U2DT-CWT transforms (as illustrated by figures III and IV) create two dimensional transforms each with 6 oriented complex subbands at each scale. The one dimensional versions of these transforms are overcomplete leading to considerable overcompleteness in two dimensions. The relative sizes of the produced subbands are illustrated in figure 3. This figure shows that both the U1DT-CWT and U2DT-CWT transforms have consistent subband sizes although as the U1DT-CWT does not contain any down-sampling it is considerably more overcomplete than both the U2DT-CWT and DT-CWT transforms.

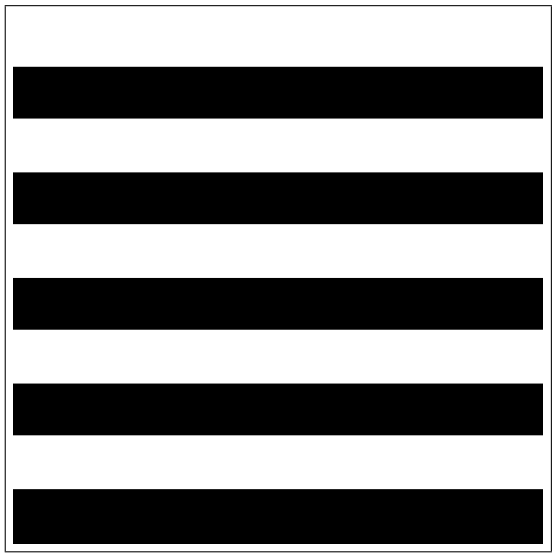

Fig. 4. Grating image (512×512) used to evaluate cross scale correlation

.

VII. Cross Scale Subband Correlation

The correlation between co -located subband coefficients at adjacent scales is a key attribute of wavelet transforms exploited within many denoising, segmentation and fusion applications (e.g. [5] [6]). As a parent subband of a decimated transform will be half the size of the considered subband, an exact one-to-one cross scale relationship will not exist between scales. The parent subband is therefore often upsampled. This will have a adverse affect on the cross scale correlation exploited within these applications. In order to examine this issue we have extracted the correlation coefficients between the third and fourth scale of the U1DT-CWT, U2DT-CWT and the DT-CWT. For the DT-CWT, the fourth scale is upsampled using simple interpolation.

VIII. Statistical Models of Wavelet Coefficients

The statistics of wavelet coefficients have found to give heavy tail distributions. These distributions have been found

Fig. 5. Lena (512×512)

.

to be better modelled using more general distributions such as the Symmetric alpha Stable (SαS) model rather than normal distributions [8].

A. The Cauchy Distribution

There is no compact expression of the Symmetric alpha Stable (SαS) distribution's PDF, making it difficult to use for denoising applications. However, a simplified version of the (SαS) distribution, the Cauchy distribution, does have a simple expression for the PDF but it also retains the ability to model the heavy tailed wavelet subband coefficients. A univariate Cauchy distribution has a PDF defined as:

$$P_\gamma(x) = \frac{1}{\pi}\left[\frac{\gamma}{x^2+\gamma^2}\right]. \tag{15}$$

where γ is the dispersion parameter that determines the spread of the distribution. The bivariate Cauchy distribution has a PDF defined as a function of it's two variables x_1 and x_2 together with a similarly defined dispersion parameter γ

$$P_\gamma(x_1,x_2) = \frac{\gamma}{2\pi\left(x_1^2+x_2^2+\gamma^2\right)^{3/2}}. \tag{16}$$

IX. Bivariate Shrinkage

Isolating each orientation of the each transform (DT-CWT, U1DT-CWT and U2DT-CWT) the coefficients at scale l and its parent subband at scale $l+1$ can be modelled in vector form as:

$$\boldsymbol{y} = \boldsymbol{x} + \boldsymbol{\epsilon} \tag{17}$$

where $\boldsymbol{y} = (y_l, y_{l+1})$ is a vector of the observed (noisy) coefficients at scale l and it's co-located coefficient at the same orientation and parent subband at scale $l+1$. Similarly $\boldsymbol{x} = \boldsymbol{\epsilon} = (\epsilon_l, \epsilon_{l+1})$ and (x_l, x_{l+1}) are defined for the noise values and denoised coefficients respectively.

TABLE I
SHIFT VARIATION (DEG) OF REAL ($\Re$), IMAGINARY ($\Im$) AND MAGNITUDE OF 1D TRANSFORMS ($M = 1024, N = 16$)

		DWT	DT-CWT			U1DT-CWT			U2DT-CWT		
			$\Re$	$\Im$	Mag	$\Re$	$\Im$	Mag	$\Re$	$\Im$	Mag
Subband Scale	1	0.7193	0.7193	0.7193	1.0000	1.0000	1.0000	1.0000	0.7193	0.7193	1.0000
	2	0.1633	0.1972	0.1972	0.9738	1.0000	1.0000	1.0000	0.2164	0.2164	1.0000
	3	0.1732	0.4967	0.4967	0.9299	1.0000	1.0000	1.0000	0.8261	0.8261	1.0000
	4	0.1749	0.5052	0.5052	0.9693	1.0000	1.0000	1.0000	0.9829	0.9829	1.0000

TABLE II
CO-LOCATED COEFF CORRELATION BETWEEN SCALES 3 & 4.

	Figure 4 (Grating)						Figure 5 (Lena)					
Subband Orientation	1	2	3	4	5	6	1	2	3	4	5	
U1DT-CWT	0.9811	0.9381	0.9381	0.9811	0.9381	0.9381	0.7195	0.7376	0.6810	0.7276	0.7265	0.7103
U2DT-CWT	0.9738	0.9101	0.9101	0.9738	0.9101	0.9101	0.7027	0.7259	0.6736	0.7148	0.7189	0.6891
DT-CWT	0.9749	0.7700	0.7700	0.9749	0.7700	0.7700	0.6486	0.6582	0.6273	0.6624	0.6641	0.6844

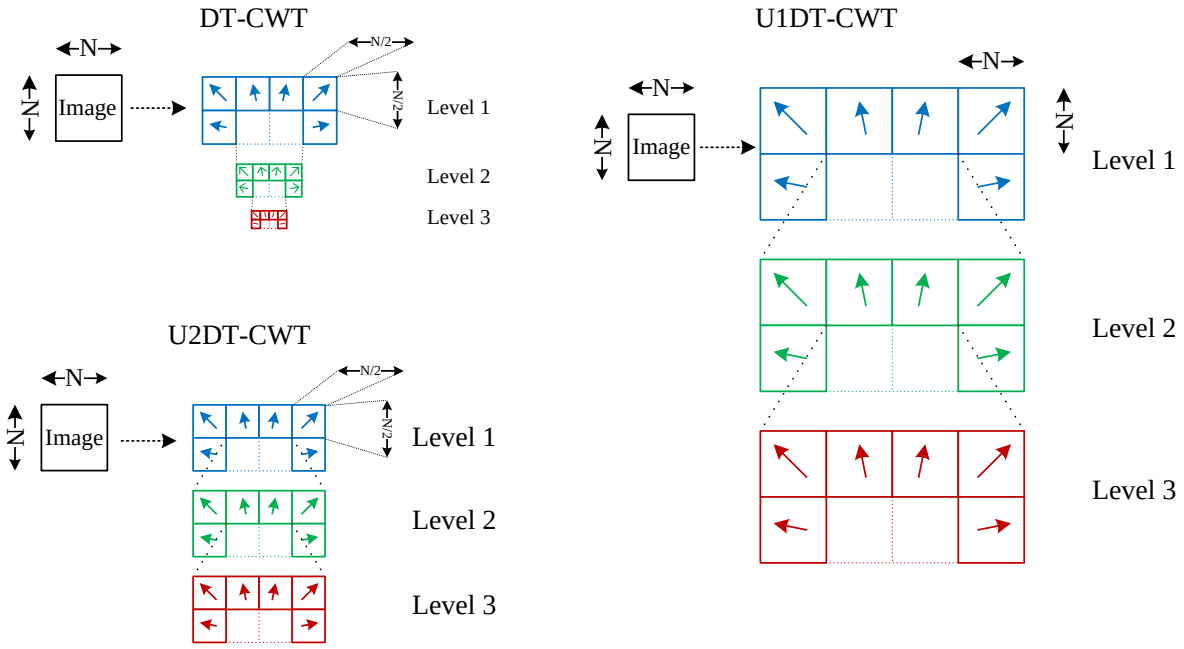

Fig. 3. Comparison of the DT-CWT, U1DT-CWT and U2DT-CWT two dimensional transforms' subbands' sizes

.

A Maximum A-Posteriori estimator of the denoised coefficients $\boldsymbol{x}$ given the observed coefficients $\boldsymbol{y}$ is defined as [5]

$$\hat{\boldsymbol{x}}(\boldsymbol{y}) = \arg\max_{x} P_{x|y}(\boldsymbol{x}|\boldsymbol{y}). \tag{18}$$

Using Bayes' theorem, this equation can be rewritten as (the noise in the subbands is assumed to be white following the assumption that noise in the image is white):

$$\begin{aligned}\hat{\boldsymbol{x}}(\boldsymbol{y}) &= \arg\max_{x} [P_{\epsilon}(\boldsymbol{y}-\boldsymbol{x})P_{\boldsymbol{x}}(\boldsymbol{x})] \\ &= \arg\max_{x} [\log(P_{\epsilon}(\boldsymbol{y}-\boldsymbol{x})) + \log(P_{\boldsymbol{x}}(\boldsymbol{x}))] \end{aligned} \tag{19}$$

$$= \arg\max_{x} \left[\frac{-(y_l - x_l)^2 - (y_{l+1} - x_{l+1})^2}{2\sigma^2} + \log(P_{\boldsymbol{x}}(\boldsymbol{x}))\right] \tag{20}$$

Therefore the problem of obtaining x_l from equation 20 involves simply solving the partial differential equations for x_l+1 and x_l of this equation [9]. The estimated clean wavelet coefficients at scale l (x_l) can be obtained from the noisy observations y_l and y_{l+1} and the estimated model parameters thus

$$x_l = \frac{y_l}{3} + t + s \tag{21}$$

where

$$t = \sqrt[3]{-\frac{q}{2} - \sqrt{\frac{p^3}{27} + \frac{q^2}{4}}}$$
$$s = \sqrt[3]{-\frac{q}{2} + \sqrt{\frac{p^3}{27} + \frac{q^2}{4}}}$$
$$q = -\frac{2y_l^3}{27} + \frac{y_l}{3}\frac{\gamma^2 + 3\sigma^2}{1 + y_{l+1}^2/y_l^2} - \frac{\gamma^2 y_l}{1 + y_{l+1}^2/y_l^2}$$
$$p = \frac{\gamma^2 + 3\sigma^2}{1 + y_{l+1}^2/y_l^2} - \frac{y_l^2}{3}$$

The derivation of these equations uses Cardano's method described by Tao et al. [9]. The model parameters γ and σ are estimated using methods discussed in section IX-A.

A. Cauchy Distribution Model Parameter Estimation

As defined by Donoho et al. [10], an estimate of the noise standard deviation (σ) in any wavelet decomposition can be calculated using the median absolute deviation (MAD) of wavelet coefficients (y_l) from one of the subbands at the first level of decomposition:

$$\hat{\sigma} = \frac{\text{MAD}(y_l)}{0.6745} \tag{22}$$

The dispersion parameter γ of equations 21 and 16 are estimated using a method based on an empirical characteristic function as proposed by Wan et al. [9]. The estimate of γ is given by the equation

$$\hat{\gamma} = -\frac{\log\varphi_y^2(\omega) - \sigma^2|\omega|^2}{2|\omega|} \tag{23}$$

where σ is the standard deviation of the noise (given by the estimate $\hat{\sigma}$ within equation 22). $\varphi_y(\omega)$ denotes the empirical characteristic function of noisy observation $\boldsymbol{y}$. ω can take any non-zero value in principle. As described within [9] the mean of the results of the estimates given by a small range of values of ω is taken as the final estimate $\hat{\gamma}$. The observed coefficients' ($\boldsymbol{y}$) PDF is the convolution of the PDFs of the noise $\boldsymbol{\epsilon}$ and the signal $\boldsymbol{x}$. Therefore, the characteristic function of the observations the product of the characteristic functions of $\boldsymbol{\epsilon}$ and $\boldsymbol{x}$. This corresponds to the equation

$$\varphi_y(\omega) = \exp(-\gamma|\omega|)\exp\left(-\frac{\sigma^2}{2}|\omega|^2\right). \tag{24}$$

X. Bivariate Shrinkage using Cauchy Model and the U1DT-CWT, U2DT-CWT transforms

A. Local Estimation of Model Parameters

The Cauchy model parameters σ and γ are estimated from equations 22, 23 and 24. However, due to the non-stationary nature of natural images, this is done on a local basis where the image statistics are assumed to be locally stationary i.e. for the coefficient to be denoised, a fixed window surrounding it's location is used to estimate the model parameters. There is a necessary trade off between the need to have a window size that captures approximate stationary statistics and the requirement to have sufficient observations to efficiently estimate the parameters locally. As the scale of the subband is increased within the decimated DT-CWT, a larger and larger spatial support is required for the same number of neighbours. As the undecimated transform has no reduction in spatial size of the subbands from scale to scale, the local estimation of the parameters can be achieved with both more localised support and/or more neighbours for estimation.

The estimated parameters σ and γ can be used in equation 21 to perform the wavelet shrinkage for each wavelet coefficient with reference to their parent. As there is no exact one-to-one relationship for co-located coefficients in the decimated DT-CWT, the observation y_{l+1} is obtained through upsampling (by a factor of 2 in each direction) the corresponding subband at scale $l+1$. Conversely, all the subbands of the undecimated transforms are all of the same size and therefore there is no need for the approximation given by the upsampling. Additionally, each coefficient observation y_l at scale l has an exact co-located coefficient y_{l+1} at scale $l+1$.

XI. Results

Two test images (Lena and boats) were denoised by first adding white noise of increasing standard deviation σ (5,10,15,20 and 25). The denoising results for each transform were compared to the original image using PSNR. The results for the proposed transforms (U1DT-CWT and U2DT-CWT) were compared to a similar bivariate denoising technique implemented using a decimated DT-CWT [5] as illustrated by table III. A window of 15×15 pixels was used for local parameter estimation for all transforms. For further comparison, the results in [5] also show a wide comparison of the DT-CWT denoising method to a range of (inferior) techniques. Table III shows the improvement in qualitative results of up to 0.4 db across the range of σ values (when comparing the DT-CWT and the U1DT-CWT). The comparison of DT-CWT and the U2DT-CWT gives a slightly smaller improvement. The improvement was assumed to be because of the improved inter scale correlation and perfect shift invariance of the transforms.

Figure 6 shows some denoising results (of the DT-CWT and U1DT-CWT transforms) for two cropped regions of the Lena image (σ = 25). It can be observed that the proposed method offers better definition for high frequency regions whilst reducing the PSNR difference between the original and the denoised image. In particular, the retention of edges is more localised compared to the decimated version (due to the denoising artefacts being more localised within the undecimated transform). This can be directly seen on the edge of the hat in figures 6(i) and 6(j) where the difference between the denoised versions and the original is more localised when using the U1DT-CWT. Furthermore, there is less ringing caused by edges (as can be observed under the left eye in figure 6(c) compared to 6(d)) and the textured areas have less noise within them when using the undecimated method. The U2DT-CWT also gives similarly improved visual results compared to the DT-CWT.

TABLE III
DENOISING RESULTS

	Barbara					Lena				
σ (Std of added noise)	**5**	**10**	**15**	**20**	**25**	**5**	**10**	**15**	**20**	**25**
DT-CWT (Achim et al. [5])	36.47	32.33	30.21	29.05	28.14	38.44	34.30	31.93	30.50	29.32
U1DT-CWT	36.70	32.58	30.47	29.23	28.31	38.60	34.50	32.09	30.69	29.49
U2DT-CWT	36.51	32.46	30.34	29.16	28.21	38.46	34.37	32.03	30.63	29.37

TABLE IV
2D WAVELET TRANSFORM COMPARISON CHART

	Advantages	**Disadvantages**	Example number of Coeffs Image size=256×256, 3 scales	
DWT	Critical decimation.	Maximum shift variance. No complex coefficients. Lack of directional selectivity.	65536	(**1**$\times 256 \times 256$)
UDWT	Perfect shift invariance. One-to-one cross scale coeff relationship	No complex coefficients. Lack of directional selectivity. Very overcomplete.	655360	(**10**$\times 256 \times 256$)
DT-CWT	Directional selectivity.	Only approximate shift invariance.	131072	(**2**$\times 256 \times 256$)
U1DT-CWT	Perfect shift invariance. One-to-one cross scale coeff relationship Directional Selectivity.	Very overcomplete.	1310720	(**20**$\times 256 \times 256$)
U2DT-CWT	Perfect shift invariance. One-to-one cross scale coeff relationship Directional selectivity. Reduced overcompleteness compared to U1DT-CWT.	Subbands not same size as image.	327680	(**5**$\times 256 \times 256$)

XII. COMPARISON OF TRANSFORMS

Table IV shows a comparison of the DWT, UDWT, DT-CWT, U1DT-CWT and U2DT-CWT transforms. The last column of this table illustrates an example number of coefficients of the transforms. It can seen that the DWT gives the most compact representation followed by the DT-CWT. However, within the denoising algorithm the DT-CWT, U2DT-CWT and U1DT-CWT transforms give progressively better objective denoising results and offer a trade-off between denoising performance and over-completeness (and therefore processing speed and memory requirements)

XIII. CONCLUSION

We propose two new undecimated versions of the dual tree complex wavelet transform: U1DT-CWT and U2DT-CWT. Firstly, the transform adds improved directionality and phase information compared to the undecimated wavelet transform. Both transforms also offer exact rather than approximate translational invariance compared to the decimated DT-CWT. Additionally, they both have the advantage of a one-to-one relationship between co-located coefficients in different subbands. Furthermore the correlation between child and parent coefficients is improved with the new transforms compared to the DT-CWT.

All of these attributes have exploited here within a denoising algorithm where the exact parent (rather than an interpolated parent) of a coefficient to be denoised is used within a bivariate shrinkage system. Additionally, without any subsampling, the estimation of the model parameters within each subband of the U1DT-CWT can be achieved on a much more local basis compared to the decimated version (while also retaining sufficient observations to give a good parameter estimation).

Although there is a large amount of statistical redundancy within U1DT-CWT and U2DT-CWT subbands, the availability of a larger number of samples at each scale and a one-to-one relationship between complex coefficients will be of use for comparative inter-subband magnitude and phase analysis in many other applications.

The described bivariate denoising application gives up to a 0.4db improvement in denoising performance when using the U1DT-CWT compared to the DT-CWT.

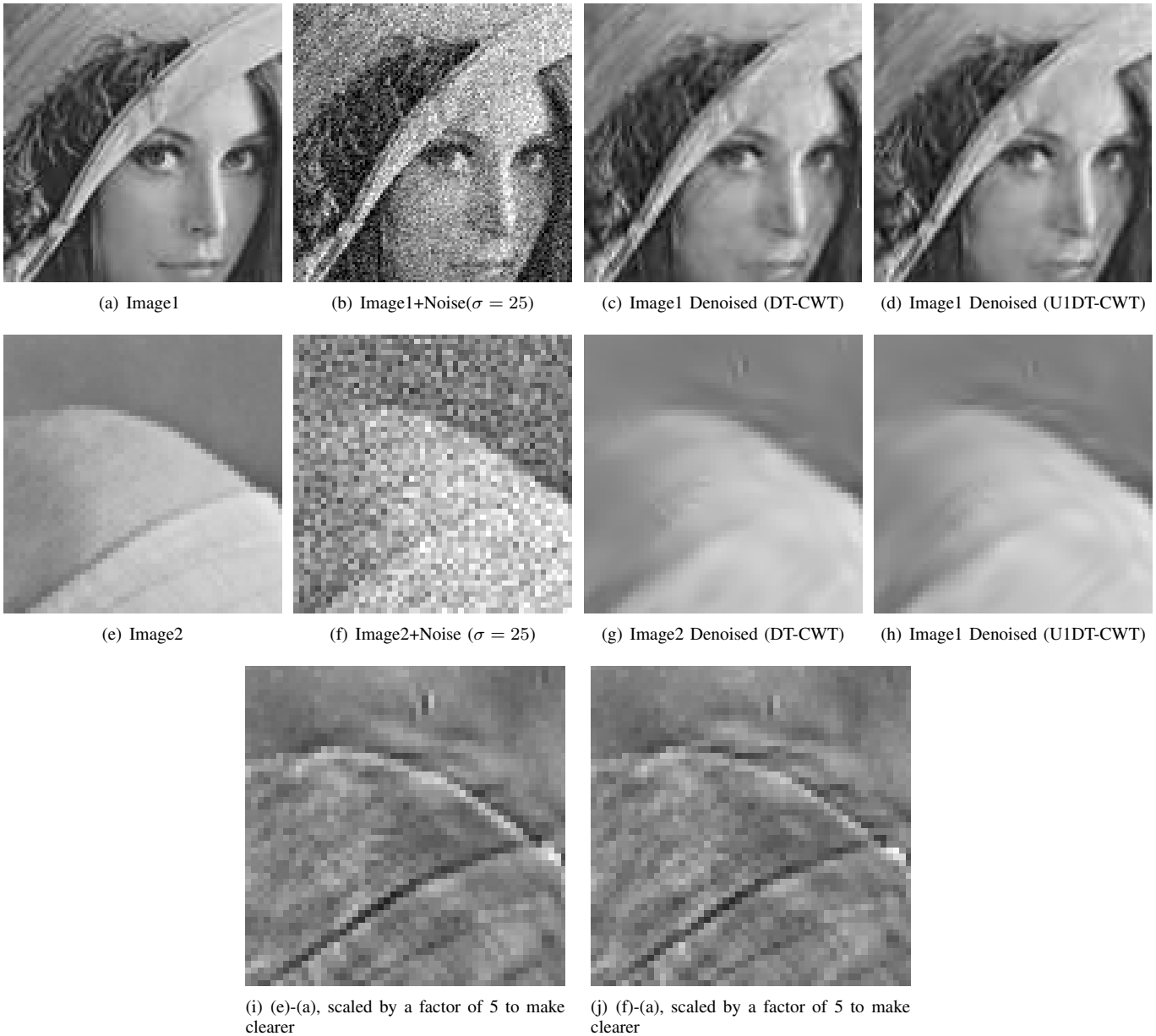

(a) Image1 (b) Image1+Noise($\sigma = 25$) (c) Image1 Denoised (DT-CWT) (d) Image1 Denoised (U1DT-CWT)

(e) Image2 (f) Image2+Noise ($\sigma = 25$) (g) Image2 Denoised (DT-CWT) (h) Image1 Denoised (U1DT-CWT)

(i) (e)-(a), scaled by a factor of 5 to make clearer

(j) (f)-(a), scaled by a factor of 5 to make clearer

Fig. 6. Denoising results

REFERENCES

[1] O. Rockinger, "Pixel-level fusion of image sequences using wavelet frames," *Proceedings of the 16th Leeds Applied Shape Research Workshop.*, pp. 149–154, 1996.

[2] P. Dutilleux, "An implementation of the algorithme a trous to compute the wavelet transform," *Wavelets: Time-Frequency Methods and Phase Space*, pp. 298–304, 1989.

[3] M. Unser, "Texture classification and segmentation using wavelet frames," *IEEE Trans. Image Process.*, vol. 4, no. 11, pp. 1549–1560, 1995.

[4] I.W. Selesnick, R.G. Baraniuk, and N.G. Kingsbury, "The dual-tree complex wavelet transform," *IEEE Signal Processing Magazine*, vol. 22, no. 6, pp. 123–151, November 2005.

[5] A. Achim and E.E. Kuruoglu, "Image denoising using bivariate alpha-stable distributions in the complex wavelet domain," *IEEE Signal Processing Letters*, vol. 12, no. 1, pp. 17–20, 2005.

[6] P. Hill, "Wavelet Based Texture Analysis and Segmentation for Image Retrieval and Fusion," *PhD, Department of Electrical and Electronic Engineering, University of Bristol*, 2002.

[7] M. Oltean I. Adam and M. Bora, "A new quasi sifht invariant non-redundant complex wavelet transform," *Scientific Bulletin of the POLITEHNICA University of Timisoara*, pp. 14–18, 2006.

[8] C.L. Nikias and M. Shao, "Signal processing with alpha-stable distributions and applications," *John Wiley and Sons, New York*, 1995.

[9] T. Wan, C.N. Canagarajah, A. Achim, "Segmentation of noisy colour images using Cauchy distributions in the complex wavelet domain," *IET Image Processing*, vol. 5, no. 2, pp. 159–170, March 2011.

[10] D.L. Donoho and I.M. Johnstone, "Ideal spatial adaptation by wavelet shrinkage," *Biometrika*, pp. 425–455, 1994.

Paul Hill received his B.Sc degree from the Open University, an M.Sc degree from the University of Bristol, Bristol, U.K. and a Ph.D. also from the University of Bristol. He is currently a Research Fellow at the University of Bristol and part time lecturer. His research interests include image and video analysis, compression and fusion. He has published over 20 academic papers.

Alin Achim received the B.Sc. and M.Sc. degrees, both in electrical engineering, from "Politehnica" University of Bucharest, Romania, in 1995 and 1996, respectively and the Ph.D. in biomedical engineering from the University of Patras, Greece, in 2003. He then obtained an ERCIM (European Research Consortium for Informatics and Mathematics) postdoctoral fellowship which he spent with the Institute of Information Science and Technologies (ISTI-CNR), Pisa, Italy and with the French National Institute for Research in Computer Science and Control (INRIA), Sophia Antipolis, France. In October 2004 he joined the Department of Electrical and Electronic Engineering at the University of Bristol as a Lecturer. His current research interests span the areas of statistical signal processing with emphasis in estimation and detection theory, multiresolution algorithms with applications in remote sensing and medical imaging, image filtering and enhancement, and segmentation and classification algorithms.

David Bull received the BSc degree form the University of Exeter in 1980, the MSc degree from the University of Manchester in 1983, and the PhD degree from the University of Cardiff in 1988. He currently holds the Chair in Signal Processing at the University of Bristol, where he was the head of the Electrical and Electronic Engineering Department between 2001 and 2006. He now heads the Visual Information Laboratory and is Director of Bristol Vision Institute. In 2001, he cofounded ProVision Communication Technologies, Ltd. His current activities are focused on the problems of image and video communications and analysis for wireless, Internet, military, and broadcast applications. He has published over 400 academic papers and is a Fellow of the IEEE.